Probing of Thermal Transport in PbTe Nanocrystal Film by Time-Domain Thermoreflectance

Marek Piotrowski[1], Miguel Franco[1], Viviana Sousa[1], José Rodrigues[1], Yohei Kakefuda[2], Naoyuki Kawamoto[2], Bryan Owens-Baird[3,4], Pedro Alpuim[1,5], Kirill Kovnir[3,4], Takao Mori[2], Yury V. Kolen´ko[1]*

[1]International Iberian Nanotechnology Laboratory, Braga 4715-330, Portugal

[2]National Institute for Materials Science (NIMS), International Center for Materials Nanoarchitectonics (MANA), Tsukuba 305-0044, Japan

[3]Iowa State University, Department of Chemistry, Ames, Iowa 50011, United States

[4]Ames Laboratory, U.S. Department of Energy, Ames, Iowa 50011, United States

[5]CFUM-Centre of Physics of the University of Minho, Braga 4715-330, Portugal

ABSTRACT

Bottom-up fabrication of thermoelectric (TE) materials from colloidal nanocrystal (NC) building blocks can substantially increase their TE efficiency, e.g., by reducing lattice thermal conductivity. In this work, we first synthesized 10-nm spherical phase-pure oleate-capped PbTe NCs with narrow size distribution and employed them to fabricate the 110-nm thick films on insulating SiO_2/Si substrates. Here, we used the spin-coating with subsequent ligand exchange procedure to ensure strong coupling interactions between the NCs. Using the dark conductivity measurements, we confirmed the semiconducting behavior and the Schottky-type electrical field-dependent conductivity mechanism in the resultant thin films. We then probed the thermal transport in the thin-film by means of a time-domain thermoreflectance (TDTR) method. For this purpose, we used a customized state-of-the-art system based on a picosecond thermoreflectance instrument, which enables area-selective analysis with the spatial resolution down to 5 μm. The results show that as-fabricated PbTe NC films exhibit ultralow thermal conductivity of ca. 1.52 W m^{-1} K^{-1}. All in all, the transport properties findings suggest potential of the proposed quick and cost-effective spin-coating strategy for bottom-up fabrication of nanostructured TE films from high-quality colloidal NC building blocks.

GRAPHICAL ABSTRACT

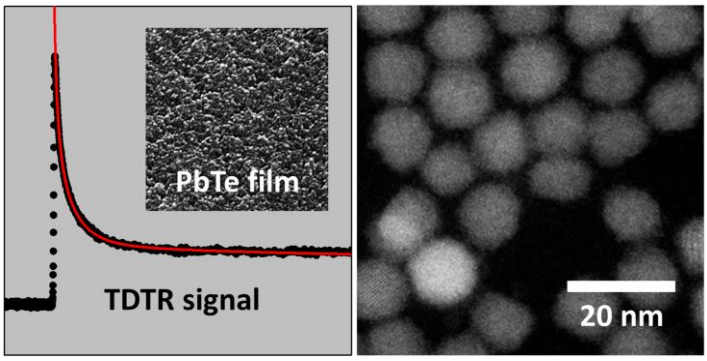

INTRODUCTION

Thermoelectric (TE) devices allow direct conversion of temperature gradient into electric current (Seebeck effect) and *vice versa* (Peltier effect), which affords an interesting avenue for energy harvesting and heat management.[1] The efficiency of TE devices is determined by Carnot efficiency and is related to the material dependent dimensionless figure of merit, $ZT = \sigma S^2 T \kappa^{-1}$, where σ is electrical conductivity, S is the Seebeck coefficient, κ is the thermal conductivity, and T is the absolute temperature. Hence, ZT is maximized in the materials that have high electrical conductivity, low thermal conductivity, and a large Seebeck coefficient. When integrated into a real device, the best bulk TE materials have $ZT \approx 1.2$, but an average $ZT = 3–4$ is necessary to make a significant impact on TE energy conversion.[2,3] Therefore, the primary goal of the research related to TE materials is to maximize their figure of merit, thus, improving the energy conversion efficiency of the resultant TE device.[4–9]

Classically, owing to intrinsic difficulties in decoupling electrons and phonons in bulk solids, the efficiency of bulk TEs continues to be insufficiently high.[10,11] Fortunately, multiple theoretical and experimental studies have indicated that creating nanostructured devices in new geometries can substantially increase TE efficiency.[12,13] In particular, new physical concepts and nanostructuring of bulk phases make it possible to modify the correlations between these bulk properties through changes in the density of states, scattering rates, and interface effects on electron and phonon transport.[14] For instance, by reducing lattice thermal conductivity through the placement of suitable nanoscale precipitates in the bulk matrix, e.g., in $AgPb_mSbTe_{m+2}$ (LAST)[15] and $NaPb_xSbTe_{2+x}$ (SALT)[16] materials, record-high-ZT values in the range of 1.5-1.8 have been achieved, but they still fall short of the generally desired range of $ZT = 3–4$.

One interesting approach to increase ZT of TE materials is top-down fabrication of nanostructured TE microdevices, which demonstrates the potential of nanostructuring to

produce, for example, extraordinarily large Seebeck coefficients in 2D electron gases[17] and altered phonon modes in patterned TE superlattices.[18] Another more cost-effective production of nanostructured TEs can be achieved via bottom-up fabrication of materials from colloidal nanocrystal (NC) building blocks.[6] It is noteworthy that bottom-up approach permits the fabrication of TE nanocomposites in a well-controlled, fast and inexpensive manner for large quantities of material, for instance, 1 μm of NC-based TE film can be obtained within just a few minutes by the spin-coating or other similar deposition routes, while it takes one day to grow a superlattice of the same thickness by the molecular beam epitaxy method. Moreover, NC building blocks are synthesized by wet chemistry, which offers the use of inexpensive and non-toxic starting materials and moderate energy-intensive processing, compared to many physical deposition techniques. Importantly, the resultant solids fabricated from nanoscale building blocks exhibit numerous relevant properties making them eligible for TE applications. Among them, the most important are the quantum confinement effect on carriers and phonons, possibility of band engineering and adjustment, as well as the efficient phonon scattering at NCs interfaces, altogether resulting in the enhanced *ZT*.[19] All in all, the investigation of bottom-up fabrication of nanostructured TEs would provide more insight into the true TE relevance of the resultant materials.

In this work, we report the colloidal synthesis and characterization of lead telluride PbTe NCs, which were used as building blocks for the fabrication of the thin films on SiO_2/Si substrate using the spin-coating technique. The structural and electron microscopy investigations of the NCs reveal that we were able to produce spherical phase-pure oleate-capped PbTe NCs with narrow size distribution at around 10 nm. After spin-coating, the films were subjected to ligand exchange procedure to ensure stronger coupling interactions between the NCs. Dark conductivity temperature-dependent studies confirm the semiconducting behavior of the resultant 110 nm thick NC films and also elucidate electrical field dependent conductivity in the films. Finally, we probed the thermal transport in the fabricated films by means of a time-domain thermoreflectance method using a customized state-of-the-art system based on a picosecond thermoreflectance instrument, which enables area-selective analysis with the resolution down to 5 μm. The results show that PbTe NC films exhibit a very low thermal conductivity of ca. 1.52 W m^{-1} K^{-1}, thereby rationalizing bottom-up approach for the fabrication of nanostructured TEs.

EXPERIMENTAL SECTION

Synthesis of colloidal PbTe NCs. PbTe NCs were obtained by the protocol adapted from that of Murphy and co-workers.[20] First, 1M tellurium precursor solution was prepared by dissolving 12.76 g (100 mmol) of elemental Te (99.99%, Alfa Aesar) in 100 mL of trioctylphosphine (TOP, 97%, Sigma-Aldrich) at 100 °C for overnight. Next, 2.25 g (10.08 mmol) of lead(II) oxide (99.9%,

Sigma-Aldrich), 12.5 mL of oleic acid (OA, 90%, Sigma-Aldrich) and 65 mL of 1-octadecene (ODE, 90%, Sigma-Aldrich) were combined in a 250 mL round-bottom flask attached to the Schlenk line. While stirring at 600 rpm, the mixture was degassed at room temperature for 30 min, and then at 90 °C for another 30 min. After switching vacuum to Ar atmosphere, the flask was heated to 150 °C, and held at this temperature for 1 h to formed lead(II) oleate complex. The flask was then cool down to 90 °C and degassed at this temperature for 30 min. After switching vacuum to Ar atmosphere, the flask was heated to 165 °C and then 10 mL of a 1M solution of Te in TOP, previously preheated to 60 °C, was quickly injected into the reaction mixture. The mixture was left to stir for 5 min at 165 °C, and then the reaction was quenched by taking off the heating mantle and rapid cooling of the flask in an ice-bath. The NCs were precipitated by the addition of absolute ethanol (99.8%, Honeywell) followed by centrifugation at 9000 rpm for 10 min. The NCs were redispersed in anhydrous hexane (99%, Sigma-Aldrich), washed with ethanol, and collected by centrifugation. After short drying *in vacuo*, the NCs were redispersed in anhydrous toluene (99.8%, Sigma-Aldrich) and subjected to centrifugation at 3000 rpm for 10 min to remove large particles and clusters. The final stock dispersion of PbTe NCs in toluene was stored in a glass vial at 4 °C.

PbTe thin-film deposition. Thin-films of PbTe NCs were fabricated by spin-coating of NC dispersion on flat SiO_2/Si substrates (1 inch × 1 inch, 100 nm thermal SiO_2 layer) adapting the reported methodology.[21] The substrates were cleaned in sequence with acetone (99.5%, Honeywell), ethanol, and isopropanol (99.8%, Honeywell) using ultrasonication for 5 min each. After drying with a gentle stream of N_2, substrates were hydrophobized by immersing them into (3-mercaptopropyl)trimethoxysilane (MPTS, 95%, Sigma-Aldrich) in toluene solution (4 μL mL^{-1}) for 12 h. Prior to the coating, the substrates were rinsed with neat toluene and dried with a gentle stream of N_2. Then, PbTe NC films were deposited. For this purposes, the stock dispersion of the NCs was firstly dried and then redispersed by sonication in octane (99%, Sigma-Aldrich) at a concentration of 30 mg mL^{-1}. 80 μL of NCs dispersion, enough to cover the 1 inch x 1 inch SiO_2/Si substrate, was distributed evenly using a micropipette to cover the entire surface of the substrate. The substrate was spun at 2000 rpm for 30 s to obtain a glassy NC film and dry the octane. Finally, the resultant NC films were subjected to ligand exchange procedure to replace native long oleate capping ligands by the short ones, in particular, the NC film was gently immersed into 10 vol.% solution of 3-mercaptopropionic acid (MPA, 99%, Sigma-Aldrich) in absolute methanol (Fisher Chemical), kept for approximately 2 s, and then steadily removed and rinsed with neat methanol. The film was dried with a gentle stream of N_2. The spin-coating and ligand exchange procedures were performed twice to increase the uniformity of the film. The resultant thin-films of PbTe NCs were stored *in vacuo* until further use.

Characterization. Powder X-ray diffraction (XRD) data were collected on an X'Pert PRO diffractometer (PANalytical) set at 45 kV and 40 mA, and equipped with Cu *K*α radiation (λ = 1.541874 Å) and a PIXcel detector. The XRD patterns were matched to International Centre for Diffraction Data (ICDD) PDF-4 database using a HighScore software package (PANalytical).

Transmission electron microscopy (TEM) and high resolution TEM (HRTEM) studies were performed using JEM 2100 microscope at 200 kV (JEOL, 0.24 nm point resolution), while high-angle annular dark field scanning TEM (HAADF–STEM) and energy-dispersive X-ray spectroscopy (EDX) in STEM mode (STEM–EDX) studies were carried out with a Titan ChemiSTEM microscope at 200 kV (FEI, 0.08 nm point resolution, Super-X EDX System). The morphology and cross sections of the PbTe NC thin-films were studied by scanning electron microscopy (SEM) using a Quanta 650 FEG ESEM microscope at 20 kV (FEI).

Dark conductivity (DC). To assess the DC properties, aluminum top electrodes (280-nm-thick and 1 mm × 1 mm in size) were deposited onto the thin-film of PbTe NCs through a ~~metal~~ shadow mask using TIMARIS FTM sputtering system (Singulus Technologies). The DC measurements were carried out using a homemade probe station dark box connected to a Keithley 6487 picoammeter/voltage source (Keithley Instruments). Both temperature and voltage were controlled using the homemade software. The temperatures were ~~ranged~~ varied in the range from 90 to 20 °C with a step of -5 °C, and after the stabilization of the temperature, the electrical current signals were recorded. The temperature-dependent conductivity, ~~(~~$\sigma(T)$, was calculated using the equation: $\sigma = I(T)l/VA$, where I is the current measured at the specific temperature T, V is the constant voltage applied to the sample, A is the cross-sectional area, and l is the distance between the electrodes. The activation energy was calculated using the Arrhenius Equation, by multiplying the slope of $\ln \sigma$ vs. $1/T$ by minus the Boltzmann constant.

Time-domain thermoreflectance. For the TDTR measurements, 100-nm-thick Pt layer was sputtered onto freshly prepared PbTe NC thin-film. The TDTR signals were corrected by using a customized system based on a PicoTR picosecond thermoreflectance instrument (PicoTherm Corp.). The customized system is capable of making area-selective analysis by focusing the spot size of the probe laser to ca. 5 μm in diameter. The thermal conductivity values of PbTe NC thin-films were estimated by using the mirror image method.[22,23] In the analytical process, the thermal interface resistance between topmost metal film and specimen is not considered.

RESULTS

Analysis of the synthesized PbTe NCs. To fabricate thin-films from NC building blocks, we first synthesized highly monodisperse 10-nm single-phase PbTe NC. Specifically, we used hot-injection colloidal synthesis method, which relays on the reacting lead(II) oleate and Te in TOP

monomer precursors at 165 °C. The resultant NCs were oleate-capped, and therefore, readily dispersible in non-polar organic solvents, such as hexane, toluene, octane, etc., forming black and transparent NC dispersions.

The synthesis of both spherical- and cubic-like colloidal PbTe NCs using a high-temperature wet chemistry approach has been first reported by Lu et.al.[24] Adapting colloidal synthesis from that of cadmium chalcogenide,[25] both spherical- and cubic-shaped PbTe NCs synthesis protocols were further optimized.[20] Later on, more focus has been directed toward further shape control and narrowing the size distribution by capping ligand mediation and changing the ligand/Pb/Te concentrations, as well as growth temperatures and durations.[26] In the current work we adapted the hot-injection colloidal synthesis of Murphy and co-workers.[20] Our results demonstrate that by adjusting the concentration of the starting precursors and oleate capping ligand while using NC growth temperature of 165 °C, we have successfully synthesized highly monodisperse single-phase nearly spherical 10-nm PbTe NCs.

We first analyzed the size and fine microstructure of the as-synthesized NCs. Figure 1a shows a representative low-magnification TEM image of the as-synthesized PbTe NCs, while the corresponding particle size distribution histogram is presented as the inset in Figure 1a. The NCs appears to be nearly spherical, and the average size of the NCs was estimated to be 10.0 ± 0.3 nm. HRTEM image evidences that the individual PbTe NCs are highly crystalline, exhibiting a well-defined crystalline structure with *d*-spacings of 3.21 Å and 2.27 Å corresponding to (200) and (220) planes of cubic PbTe (Figure 1b). Additionally, the corresponding Fourier transform (FT) pattern (inset in Figure 1b) proves that the NCs are crystalized in a cubic structure (space group *Fd*–3*m*).

We further investigated the chemical and phase composition of the resultant NCs by means of element-specific EDX mapping and XRD, respectively. HAADF–STEM images at different magnifications are shown in Figure 1c, which displays uniform in diameter NCs. The respective STEM–EDX elemental maps highlight the homogeneous distribution of Pb (Figure 1d) and Te (Figure 1e) elements in the sample, suggesting that the NCs are single-phase PbTe, devoid of any secondary phases. These results are further supported by the phase composition analysis. In particular, according to the XRD data, the as-synthesized NCs are a single-phase PbTe with a cubic structure (Figure 1f).

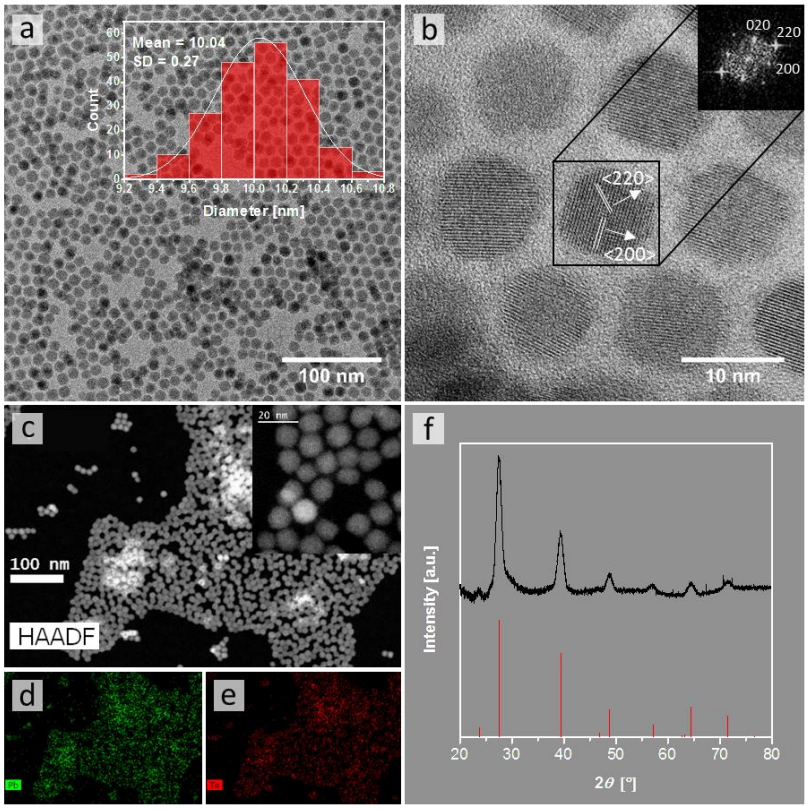

Figure 1. Low-magnification TEM image (a), particle size distribution histogram (inset in Figure 1a), HRTEM image (b) and the corresponding FT pattern (inset in Figure 1b) of the synthesized PbTe NCs. HAADF−STEM images (c) of the PbTe NCs, together with the simultaneously collected EDX maps for Pb (d) and Te (e) elements. XRD pattern of drop-casted film produced from as-synthesized PbTe NCs (f). Tick marks below the pattern correspond to the positions of the Bragg reflections expected for PbTe (ICDD no. 04-004-5888, cubic, *Fm*–3*m*).

Analysis of the PbTe NC thin-films. Having prepared high-quality PbTe NCs building blocks, we fabricated fine and well-defined 110-nm thin-films. For this purpose, we applied versatile spin-coating technique, wherein the homogeneous dispersion of PbTe NCs was deposited directly onto the hydrophobized SiO_2/Si substrate. This procedure was performed twice to achieve desired film thickness. Notably, to partially remove the native insulating long-chain oleate

capping ligands, as well as to permit for subsequent spin-coating without dispersing already deposited layer, after each spin-coating, we carried out exchange of oleate ligands with shorter propyl ones via immersing the film into MPA solution in methanol.

Subsequently, we studied the surface morphology of as-fabricated PbTe NC thin-film. SEM images of the films before (Figure 2a) and after (Figure 2b) ligand exchange show that the films consist of individual NCs, and also demonstrate that the overall film appearance remains largely intact after MPA treatment. At the same time, one can observe that partial removal of native oleate ligands reduces interparticle spacing, which is expected to enhance the electronic coupling between the NCs. A cross-sectional SEM image of the resultant PbTe NC film is shown in Figure 2c. The 110-nm thick PbTe NC layer is clearly identified on the top of the SiO_2/Si substrate. The surface of a discrete NC film appears to be relatively smooth, and the interface between the film and the supporting substrate is quite sharp, suggesting good adhesion of the PbTe NCs to SiO_2/Si.

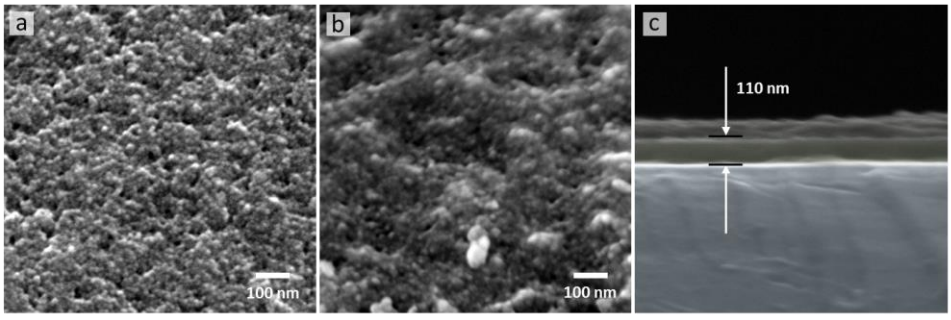

Figure 2. SEM images of the surface of the PbTe NC film before (a) and after (b) ligand exchange procedure, together with cross-sectional SEM image of the final NC film (c).

Investigation electrical transport properties of PbTe NC film. Having fabricated homogenous and densely packed thin-films of PbTe NCs, we further proved semiconducting behavior and observed electrical field-dependent conductivity in the films by means of the direct temperature-dependent dark conductivity measurements.

Bulk PbTe is a narrow band-gap semiconductor (0.32 eV) having a high melting point, good chemical stability, low vapor pressure, good chemical strength and high *ZT*.[27] The maximum *ZT* for PbTe has been reported to be 0.8–1.0 at approximately 650 K.[28] Nanostructuring of PbTe can substantially increase its thermoelectric efficiency through, e.g., quantum confinement effects, and the efficient phonon scattering at NCs interfaces in PbTe nanocrystal films,[29,30] even though such nanofabrication approach notably diminishes electrical conductivity of bulk PbTe

due to the short but critical distances between the NCs. To investigate the effect of ~~the~~ nanostructuring on the electrical transport ~~in~~ of the thin-films ~~composed of densely packed highly monodisperse PbTe NCs~~, we performed dark conductivity temperature-dependent measurements. From the reproducible dependency on temperature of the ~~temperature-dependent~~ experimental data shown in Figure 3a, we calculated the electrical conductivity at room temperature to be $\sigma_{d\,T=298\,K}$ = 5.81 × 10^{-7} S cm^{-1}, ~~as well as~~ and estimated the activation energy of the dark conductivity ~~value~~ to be E_a = 0.25 eV. The measurements were done under applied voltage V = 5 V (E_{field} = 50 V/cm). The ~~obtained~~ results confirm~~ed~~ the semiconducting behavior of as-fabricated 110-nm PbTe NC film under low bias.

Moreover, we observed that E_a ~~the activation energy~~ decreases with the increase of applied electric field (Figure 3b)~~, possibly due to the lowering of the potential barrier between the hopping sites~~. Specifically, in the low-field region below 1.5 kV cm^{-1}, the NC film exhibits semiconducting behavior, ~~exhibiting~~ with a ~~a very strong temperature dependence of~~ temperature activated ~~the~~ conductivity (Figure 3a) ~~and the activation energy~~. ~~At the same time,~~ ~~at~~At higher applied fields (~~> above~~ 1.5 kV cm^{-1})~~,~~ there is weak temperature dependence of the conductivity~~, with~~ ($|E_a|$ ~~*activation energy* below~~ < 0.~~2~~1 eV) and E_a < 0 (Figure 3b). The obtained results suggest the change of the PbTe NC films behavior from semiconducting towards metallic in the high-field region. The inset in Figure 3a ~~shows~~ plots the ln($J\,T^{-2}$) vs T^{-1} ~~plot~~ and a linear regression fitting to the Schottky emission equation~~ref~~ : ~~(~~$\ln\left(\frac{J}{T^2}\right) \sim \frac{2\beta}{T}$ ~~eq. 1)~~,

$\beta = -e\left(\phi_b - \sqrt{\frac{eE_{field}}{4\pi\varepsilon\varepsilon_0}}\right)$ where ϕ_b is barrier height, e is elementary charge, ε is dielectric constant of the material, and ε_0 is vacuum permittivity. The ~~with a high~~ coefficient of ~~determination~~ correlation is 0.998, thus confirming the Schottky emission mechanism.

~~$J = A \times T^2 \exp\left[\frac{-e\left(\phi_b - \sqrt{\frac{e\frac{V}{d}}{4\pi\varepsilon_i}}\right)}{kT}\right]$ (eq. 1)~~

~~$\ln\left(\frac{J}{T^2}\right) \sim \frac{2\beta}{T}$ (eq. 2)~~

~~$\ln(J) \sim 2\beta V^{\frac{1}{2}}$ (eq. 3)~~

Formatada: Tipo de letra: Itálico

Código de campo alterado

Comentado [PA1]: Ref: Orloff, J. (2008). "Schottky emission". *Handbook of Charged Particle Optics* (2nd ed.). CRC Press. pp. 5–6. ISBN 978-1-4200-4554-3.

Código de campo alterado

Código de campo alterado

Código de campo alterado

Código de campo alterado

~~Besides the shift of activation energy at the higher electric field from positive to negative values, the measured data is coherent with Schottky emission equation.~~ Figure 3c and Figure 3d ~~(together with insets)~~ show *I*–*V* sweeps performed ~~for~~ at low and high electric field~~s regions~~, respectively, and the corresponding fittings (insets) to the ~~temperature and~~ voltage dependencies: $\ln J \propto 2\beta\sqrt{V}$ ~~(eq. 2 and eq. 3)~~. Regardless of the range where the applied electric field ~~applied~~falls, Schottky emission equation provides the best fit to the collected data with a coefficient of ~~determination~~ correlation of ~~higher than~~ 0.94 or higher~~6~~.

Código de campo alterado

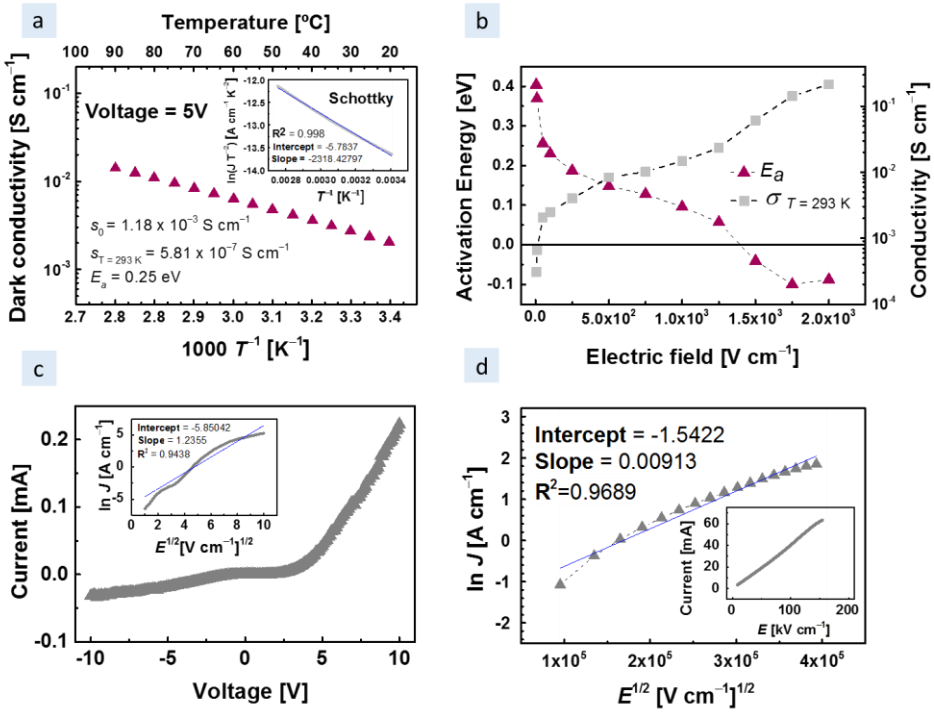

Figure 3. (a) Arrhenius plot of the ~~D~~dark conductivity of PbTe NC film measured at ~~the~~ a fixed ~~applied field~~ voltage ~~while varying~~as a function of ~~the~~ temperature. The inset shows a linear regression fitting of the data to the Schottky emission equation, ~~together with the corresponding Arrhenius plot (a) and~~ $\ln(J\,T^{-2})$ vs T^{-1} ~~plot with linear regression fitting to the Schottky emission equation (inset in Figure 3a)~~. (b) Activation energy (red triangles) and conductivity (gray squares) plotted as a function of the applied electric field ~~for PbTe NC film~~

~~(b)~~. (c) *I–V* characteristics ~~in~~ under ~~the~~ low bias~~ field region.~~ ~~(c)~~ (d) *I–V* characteristics under high bias. Insets show fittings to the Schottky emission equation, ~~with the corresponding~~ ln*J* vs $E^{1/2}$ ~~plot fitted to the Schottky emission equation (inset in Figure 3c). ln*J* vs $E^{1/2}$ plot at the higher electric field with the corresponding fitting to the Schottky emission equation (d) and the respective *I–E* sweep (inset in Figure 3d)~~.

Evaluation of thermal transport properties of PbTe NC film.

We used customized state-of-the-art TDTR system to measure the thermal conductivity of as-fabricated semiconducting thin film of PbTe NCs, and the value of the room temperature thermal conductivity was estimated to be 1.52 watts per meter per degree kelvin (W m^{-1} K^{-1}).

For narrow band-gap semiconductors like bulk PbTe, the thermal conductivity is strongly influenced by the non-parabolic nature of the energy bands[27] and is approximately 2.2 W m^{-1} K^{-1} at room temperature, and decreases at higher temperatures as a function of T^{-1}.[28] Nanostructuring of PbTe can substantially decrease the thermal conductivity of the material, and accordingly significantly enhance *ZT*.

To probe the thermal transport properties in our nanostructured PbTe thin-films, we used a picosecond thermoreflectance instrument enabling area-selective analysis with the spatial resolution down 5 μm. Such resolution was a prerequisite to obtaining an excellent data even though some macro-scale inhomogeneity at the film surface was observed (Figure 4a). Figure 4b shows TDTR signal measured for the thin-film of PbTe NCs after subtracting the baseline offset value. The fitting curve of the mirror image method is presented as a red line. By using density and specific heat values of 8.16 g cm^{-3} and 156 J kg^{-1} K^{-1}, we estimated the measured thermal conductivity to be 0.91 W m^{-1} K^{-1}.

Afterward, we assumed that the void fraction between randomly organized PbTe NCs in the film is 0.4. The volume fraction of random-close packing of highly monodisperse hard spheres typically occurs close to 0.64,[31] however the presence of propyl surfactants on the NCs surface should be taken into account.[32] It has been shown that exchanging the oleic acid ligands to shorter one (N_2H_2) increased the core volume fraction for PbS nanocrystal film after spin coating from 0.43 to 0.61.[30] Due to the very large void fraction the phonon-pore scattering is negligible, thus, the actual thermal conductivity can be estimated to be ca. 1.52 W m^{-1} K^{-1}.

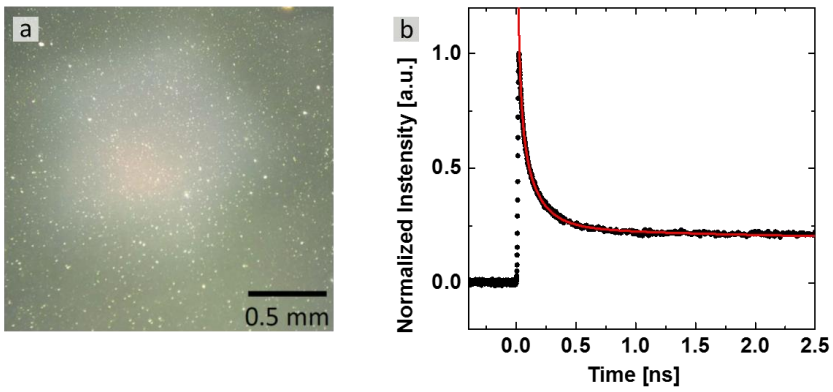

Figure 4. Optical microscopy image of the surface of the thin-film of PbTe NCs after Pt deposition (a). TDTR signal recorded for thin-film of PbTe NCs after subtracting background baseline and normalizing; red line indicates the fitting result by using the mirror image method (b).

DISCUSSION

Numerous PbTe-based nanomaterials have been fabricated using various fabrication techniques. For example, films with nanometer-scale thickness were successfully prepared by electrodeposition,[33] vacuum deposition,[34] or molecular beam epitaxy,[35] while the wafer-scale pattered nanowire thin arrays were obtained through lithographically patterned electrodeposition.[36] Nonetheless, only few works have been reported for the fabrication of PbTe thin-films from individual NCs and the evaluation of their transport properties. For instance, PbTe NC films were prepared by drop-casting NC dispersion in hexane/octane mixture on thin microscope cover glass.[29] In another study, PbTe arrays were formed by spin-casting concentrated colloidal solutions of individual nanocrystals.[30]

Before we discuss our results on transport properties of as-fabricated PbTe NC films, we will refer to the properties of the bulk and nanostructured PbTe, ranked among fundamental thermoelectric materials. In brief, the band gap of bulk homogenous PbTe is 0.32 eV and the maximum *ZT* reported to be 0.8–1.0 at approximately 650 K,[28] thus marking the applicability of this material for power generation applications. Novel concepts of nanostructuring of PbTe bulk phases include the modification of the density of states, scattering rates, and interface effects on electron transport.[14] Harman et al. reported that the *ZT* at 300 K could be doubled from 0.45 to 0.9 for PbTe and PbSeTe/PbTe superlattices fabricated using molecular beam epitaxy.[37,38] It

has been also reported that the distortion of the electronic density of states through the implementation of impurities in PbTe phase results in almost twofold increase of *ZT* to above 1.5 at 773 K.[39] These experimental results on defect states have been further confirmed theoretically using density functional theory and supercell models.[40] Notably, a combination of bottom-up nanostructuring and employing high-quality monodisperse NC building blocks sharpens the distribution of the density of states of the resultant PbTe NC solid, leading to the increase of the Seebeck coefficient.[29] Additionally, narrowing the size distribution of the NC bulding blocks also increases the electrical conductivity by reducing energy level variations.[29] It has also been demonstrated that following this approach similar PbSe NC solids exhibited a Seebeck coefficient in the range 700-1150 μV K^{-1} for PbTe nanocrystals diameter from 8.6-4.8 nm, respectively, thus for comparable carrier concentrations in bulk PbSe the enhancement is of several hundred microvolts per kelvin.[41]

~~We investigate the electrical transport properties of our thin-films of PbTe NCs by DC temperature-dependent measurements.~~ The results of dark conductivity measurements as a function of temperature confirm semiconducting behavior of PbTe nanostructured films ~~in~~ under ~~the~~ low bias ~~field region~~. Compared with continuous films deposited in vacuum and annealed, which have E_a = 0.125 eV and 0.118 eV for thickness of 50 nm and 220 nm, respectively,[34] ~~Further we have found that the activation energy of~~ our PbTe NC films have lower and highly field-dependent activation energy (0.19 < E_a < 0.40 eV for 250 > E > 5 V/cm, respectively)~~as-fabricated film E_a = 0.25 eV, which is approximately two times higher than E_a of PbTe films obtained using vacuum deposition and annealing route (0.125 eV and 0.118 eV for films with a thickness of 50 nm and 220 nm, respectively).[34]~~ The room temperature ~~electrical~~ dark conductivity of our films ~~at room temperature~~ is in the range $3.10 \times 10^{-4} < \sigma_{dT=298\,K} <= 5.814.01 \times 10^{-3}$~~7~~ S cm^{-1}. The reported value of electrical conductivity of hot-pressed PbTe nanocrystals is 3.2 S cm^{-1} at 300 K[42] while PbTe single crystals grown by the Bridgman method is 32 S cm^{-1} at 300 K.[43] The ~~N~~nanofabrication approach notably diminishes the electrical conductivity of PbTe due to ~~the short but critical distances between~~the discrete nature of NCs in the films ~~the NCs.~~. ~~Therefore~~ The ligand exchange procedure, sortening or removing organic moieties between NCs, is critical for boosting the interparticles interaction in the solids constructed from NC building blocks.[44–46] For instance, it is reported that replacing hydrophobic organic ligands by highly charged inorganic ones may increase the electrical conductivity in the film by several orders of magnitude, which is mainly due to the overlapping and coupling of the NC and ligand vibrational states.[30] As an example, a 10 order of magnitude increase in electrical conductivity (to ~8.5 S cm^{-1}) was obtained for thin films of PbSe through temperature annealing and subsequent ligand removal by hydrazine soaking.[47] It should be also taken into account that low electrical conductivity of the PbTe NC film can be attributed to the the fact

that surface of PbTe NCs may slightly oxidize[48] influencing the electrical ~~resistivity~~ transport ~~of~~ in the films.[49]

Our results further demonstrate the changes in the material from semiconducting, under low electric field, towards metallic behavior, ~~when the~~under high ~~electric~~ field ~~was applied~~. This observation is consistent with data reported by Kungumadevi and co-workers, who studied the dependence of the conductivity of PbTe film fabricated by vacuum thermal evaporation ~~over~~ on the applied electric field ~~applied~~ and observed ~~the~~ similar field-dependent behavior.[34] From the direct temperature-dependent DC measurements, collectively, our results demonstrate that the dominant electrical transport mechanism describing both temperature and electrical field-dependent conductivity of our films can be rationalized by a field-assisted Schottky emission model, wherein the electrons can obtain enough energy to overcome the ligand energy barrier and be injected into the conduction band of the PbTe.

In general, nanostructuring of bulk PbTe, in contrast to the unfavorable reduction of electrical conductivity, can substantially decrease its thermal conductivity, and hence notably enhance its overall thermoelectric *ZT*.[29,30] We measured thermal conductivity and estimated its value to be 0.91 W m^{-1} K^{-1}. Assuming that the void fraction in the PbTe thin film is 0.4, the phonon-pore scattering was considered negligible beyond the volume effect.[50] Therefore, the actual thermal conductivity can be estimated at 1.52 W m^{-1} K^{-1}. For bulk PbTe, the thermal conductivity is approximately 2.2 W m^{-1} $K^{-}1$ at room temperature,[28,51] thus, our approach in nanostructuring of PbTe contributes to the significant reduction of its thermal conductivity by a factor of around 30%. This effect appears to be similar range but slightly larger as compared to those previously reported on PbTe-based nanostructuring materials, such as 1.66-1.94 W m^{-1} $K^{-}1$ for $PbS_{1-x}Te_x$ (x=0.03-0.16),[52] 1.6-2.1 W m^{-1} K^{-1} for $PbTe_{1-x}Se_x$ (x=0-0.1).[53] Smaller thermal conductivities have been reported for PbTe nanowires, 1.3 W m^{-1} K^{-1},[54] and PbSeTe nanoparticles.[55]

CONCLUSIONS

In conclusion, we have estimated thermal conductivity of the 110-nm thin semiconducting film fabricated by spin-coating highly monodisperse single-phase nearly spherical 10-nm lead telluride nanocrystals at approximately 1.52 W m^{-1} K^{-1}. Therefore, we proved that our approach for bottom-up nanostructuring of PbTe films significantly reduces the thermal conductivity of bulk PbTe to a similar range as compared to previously reported PbTe-based nanomaterials. The results denote the potential usefulness of the proposed fast and inexpensive spin-coating strategy for bottom-up fabrication of PbTe thin films from high-quality colloidal nanocrystal building blocks, for e.g., TE applications.

AUTHOR INFORMATION

Corresponding Author

Comentado [PA2]: Wasn't this confirmed by XPS in our films? If so, it should be stated by adding a sentence here.

*(Yury V. Kolen´ko) E-mail: yury.kolenko@inl.int

ORCID

Marek Piotrowski: 0000-0002-1075-328X
Yury V. Kolen´ko: 0000-0001-7493-1762

Author Contributions

The manuscript was written through contributions of all authors. All authors have given approval to the final version of the manuscript.

Notes

The authors declare no competing financial interest.

ACKNOWLEDGMENTS

M.P. would like to acknowledge INL for post-doctoral fellowship and thank Dr. E. Carbó-Argibay for his fruitful scientific and technical input on electron microscopy. This work was supported by FROnTHERA (NORTE-01-0145-FEDER-000023) project co-financed by European Union Funds, through Portuguese NORTE 2020 programme.

REFERENCES

(1) Bell, L. E. Cooling, Heating, Generating Power, and Recovering Waste Heat with Thermoelectric Systems. *Science (80-.).* **2008**, *321* (5895), 1457 LP-1461.

(2) Rowe, D. M. *CRC Handbook of Thermoelectrics*; CRC Press, 1995.

(3) Nanoengineering Thermoelectrics for 21st Century: Energy Harvesting and Other Trends in the Field. *Renew. Sustain. Energy Rev.* **2013**, *24*, 288–305.

(4) Urban, J. J. Prospects for Thermoelectricity in Quantum Dot Hybrid Arrays. *Nat Nano* **2015**, *10* (12), 997–1001.

(5) Ziabari, A.; Zebarjadi, M.; Vashaee, D.; Shakouri, A. Nanoscale Solid-State Cooling: A Review. *Reports Prog. Phys.* **2016**, *79* (9), 95901.

(6) Ortega, S.; Ibanez, M.; Liu, Y.; Zhang, Y.; Kovalenko, M. V; Cadavid, D.; Cabot, A. Bottom-up Engineering of Thermoelectric Nanomaterials and Devices from Solution-Processed Nanoparticle Building Blocks. *Chem. Soc. Rev.* **2017**, *46* (12), 3510–3528.

(7) Owens-Baird, B.; Heinrich, S.; Kovnir, K. Thermoelectric Materials. In *Encyclopedia of Inorganic and Bioinorganic Chemistry*; John Wiley & Sons, Ltd, 2017; pp 1–35.

(8) He, J.; Tritt, T. M. Advances in Thermoelectric Materials Research: Looking Back and Moving Forward. *Science (80-.).* **2017**, *357* (6358).

(9) Zeier, W. G.; Zevalkink, A.; Gibbs, Z. M.; Hautier, G.; Kanatzidis, M. G.; Snyder, G. J. Thinking Like a Chemist: Intuition in Thermoelectric Materials. *Angew. Chemie Int. Ed.* **2016**, *55* (24), 6826–6841.

(10) DiSalvo, F. J. Thermoelectric Cooling and Power Generation. *Science (80-.).* **1999**, *285* (5428), 703–706.

(11) Pei, Y.; Wang, H.; Snyder, G. J. Band Engineering of Thermoelectric Materials. *Advanced Materials*. 2012.

(12) Boukai, A. I.; Bunimovich, Y.; Tahir-Kheli, J.; Yu, J.-K.; Goddard III, W. A.; Heath, J. R. Silicon Nanowires as Efficient Thermoelectric Materials. *Nature* **2008**, *451*, 168.

(13) Hicks, L. D.; Dresselhaus, M. S. Effect of Quantum-Well Structures on the Thermoelectric Figure of Merit. *Phys. Rev. B* **1993**, *47* (19), 12727–12731.

(14) Biswas, K.; He, J.; Blum, I. D.; Wu, C.-I.; Hogan, T. P.; Seidman, D. N.; Dravid, V. P.; Kanatzidis, M. G. High-Performance Bulk Thermoelectrics with All-Scale Hierarchical Architectures. *Nature* **2012**, *489*, 414.

(15) Hsu, K. F.; Loo, S.; Guo, F.; Chen, W.; Dyck, J. S.; Uher, C.; Hogan, T.; Polychroniadis, E. K.; Kanatzidis, M. G. Cubic AgPbmSbTe2+m: Bulk Thermoelectric Materials with High Figure of Merit. *Science (80-.).* **2004**, *303* (5659), 818–821.

(16) Poudeu, P. F. P.; D'Angelo, J.; Downey, A. D.; Short, J. L.; Hogan, T. P.; Kanatzidis, M. G. High Thermoelectric Figure of Merit and Nanostructuring in Bulk P-Type Na1−xPbmSbyTem+2. *Angew. Chemie Int. Ed.* **2006**, *45* (23), 3835–3839.

(17) Ohta, H.; Mizuno, T.; Zheng, S.; Kato, T.; Ikuhara, Y.; Abe, K.; Kumomi, H.; Nomura, K.; Hosono, H. Unusually Large Enhancement of Thermopower in an Electric Field Induced Two-Dimensional Electron Gas. *Adv. Mater.* **2012**, *24* (6), 740–744.

(18) Yu, J.-K.; Mitrovic, S.; Tham, D.; Varghese, J.; Heath, J. R. Reduction of Thermal Conductivity in Phononic Nanomesh Structures. *Nat. Nanotechnol.* **2010**, *5*, 718.

(19) Mao, J.; Liu, Z.; Ren, Z. Size Effect in Thermoelectric Materials. *Npj Quantum Mater.* **2016**, *1*, 16028.

(20) Murphy, J. E.; Beard, M. C.; Norman, A. G.; Ahrenkiel, S. P.; Johnson, J. C.; Yu, P.; Mićić, O. I.; Ellingson, R. J.; Nozik, A. J. PbTe Colloidal Nanocrystals: Synthesis, Characterization, and Multiple Exciton Generation. *J. Am. Chem. Soc.* **2006**, *128* (10), 3241–3247.

(21) Chernomordik, B. D.; Marshall, A. R.; Pach, G. F.; Luther, J. M.; Beard, M. C. Quantum Dot Solar Cell Fabrication Protocols. *Chem. Mater.* **2017**, *29* (1), 189–198.

(22) Baba, T. Analysis of One-Dimensional Heat Diffusion after Light Pulse Heating by the Response Function Method. *Jpn. J. Appl. Phys.* **2009**, *48* (5S2), 05EB04.

(23) Kakefuda, Y.; Yubuta, K.; Shishido, T.; Yoshikawa, A.; Okada, S.; Ogino, H.; Kawamoto, N.;

Baba, T.; Mori, T. Thermal Conductivity of PrRh4.8B2, a Layered Boride Compound. *APL Mater.* **2017**, *5* (12), 126103.

(24) Lu, W.; Fang, J.; Stokes, K. L.; Lin, J. Shape Evolution and Self Assembly of Monodisperse PbTe Nanocrystals. *J. Am. Chem. Soc.* **2004**, *126* (38), 11798–11799.

(25) Peng, Z. A.; Peng, X. Formation of High-Quality CdTe, CdSe, and CdS Nanocrystals Using CdO as Precursor. *J. Am. Chem. Soc.* **2001**, *123* (1), 183–184.

(26) Mokari, T.; Zhang, M.; Yang, P. Shape, Size, and Assembly Control of PbTe Nanocrystals. *J. Am. Chem. Soc.* **2007**, *129* (32), 9864–9865.

(27) Dughaish, Z. H. Lead Telluride as a Thermoelectric Material for Thermoelectric Power Generation. *Phys. B Condens. Matter* **2002**, *322* (1), 205–223.

(28) Kanatzidis, M. G. Nanostructured Thermoelectrics: The New Paradigm? *Chem. Mater.* **2010**, *22* (3), 648–659.

(29) Ko, D.-K.; Murray, C. B. Probing the Fermi Energy Level and the Density of States Distribution in PbTe Nanocrystal (Quantum Dot) Solids by Temperature-Dependent Thermopower Measurements. *ACS Nano* **2011**, *5* (6), 4810–4817.

(30) Ong, W.-L.; Rupich, S. M.; Talapin, D. V; McGaughey, A. J. H.; Malen, J. A. Surface Chemistry Mediates Thermal Transport in Three-Dimensional Nanocrystal Arrays. *Nat. Mater.* **2013**, *12*, 410.

(31) BERNAL, J. D.; MASON, J. Packing of Spheres: Co-Ordination of Randomly Packed Spheres. *Nature* **1960**, *188*, 910.

(32) Schapotschnikow, P.; Vlugt, T. J. H. Understanding Interactions between Capped Nanocrystals: Three-Body and Chain Packing Effects. *J. Chem. Phys.* **2009**, *131* (12), 124705.

(33) Saloniemi, H.; Kemell, M.; Ritala, M.; Leskelä, M. PbTe Electrodeposition Studied by Combined Electrochemical Quartz Crystal Microbalance and Cyclic Voltammetry. *J. Electroanal. Chem.* **2000**, *482* (2), 139–148.

(34) Kungumadevi, L.; Rajasekar, K.; Subbarayan, A.; Sathyamoorthy, R. Structural and Dc Conduction Studies on PbTe Thin Films. *Ionics (Kiel).* **2008**, *14* (1), 63–67.

(35) Ye, Z.; Cui, S.; Shu, T.; Ma, S.; Liu, Y.; Sun, Z.; Luo, J.-W.; Wu, H. Electronic Band Structure of Epitaxial PbTe (111) Thin Films Observed by Angle-Resolved Photoemission Spectroscopy. *Phys. Rev. B* **2017**, *95* (16), 165203.

(36) Yang, Y.; Taggart, D. K.; Brown, M. A.; Xiang, C.; Kung, S.-C.; Yang, F.; Hemminger, J. C.; Penner, R. M. Wafer-Scale Patterning of Lead Telluride Nanowires: Structure, Characterization, and Electrical Properties. *ACS Nano* **2009**, *3* (12), 4144–4154.

(37) Harman, T. C.; Taylor, P. J.; Spears, D. L.; Walsh, M. P. Thermoelectric Quantum-Dot

Superlattices with High ZT. *J. Electron. Mater.* **2000**, *29* (1), L1–L2.

(38) Harman, T. C.; Taylor, P. J.; Walsh, M. P.; LaForge, B. E. Quantum Dot Superlattice Thermoelectric Materials and Devices. *Science (80-.).* **2002**, *297* (5590), 2229–2232.

(39) Heremans, J. P.; Jovovic, V.; Toberer, E. S.; Saramat, A.; Kurosaki, K.; Charoenphakdee, A.; Yamanaka, S.; Snyder, G. J. Enhancement of Thermoelectric Efficiency in PbTe by Distortion of the Electronic Density of States. *Science (80-.).* **2008**, *321* (5888), 554–557.

(40) Hoang, K.; Mahanti, S. D.; Jena, P. Theoretical Study of Deep-Defect States in Bulk PbTe and in Thin Films. *Phys. Rev. B* **2007**, *76* (11), 115432.

(41) Wang, R. Y.; Feser, J. P.; Lee, J.-S.; Talapin, D. V; Segalman, R.; Majumdar, A. Enhanced Thermopower in PbSe Nanocrystal Quantum Dot Superlattices. *Nano Lett.* **2008**, *8* (8), 2283–2288.

(42) James, D.; Lu, X.; Nguyen, A. C.; Morelli, D.; Brock, S. L. Design of Lead Telluride Based Thermoelectric Materials through Incorporation of Lead Sulfide Inclusions or Ligand Stripping of Nanosized Building Blocks. *J. Phys. Chem. C* **2015**, *119* (9), 4635–4644.

(43) Todosiciuc, A.; Nicorici, A.; Condrea, E.; Warchulska, J. Effect of Magnetic Gd Impurities on the Electrical Properties of PbTe Single Crystals. *Surf. Eng. Appl. Electrochem.* **2013**, *49* (4), 312–315.

(44) L., R. E.; Raffaella, B.; Anna, L.; M., S. A.; J., M. D.; A., H. B. Exceptionally Mild Reactive Stripping of Native Ligands from Nanocrystal Surfaces by Using Meerwein's Salt. *Angew. Chemie Int. Ed.* **2011**, *51* (3), 684–689.

(45) Sanehira, E. M.; Marshall, A. R.; Christians, J. A.; Harvey, S. P.; Ciesielski, P. N.; Wheeler, L. M.; Schulz, P.; Lin, L. Y.; Beard, M. C.; Luther, J. M. Enhanced Mobility CsPbI₃ Quantum Dot Arrays for Record-Efficiency, High-Voltage Photovoltaic Cells. *Sci. Adv.* **2017**, *3* (10).

(46) Balazs, D. M.; Rizkia, N.; Fang, H.-H.; Dirin, D. N.; Momand, J.; Kooi, B. J.; Kovalenko, M. V; Loi, M. A. Colloidal Quantum Dot Inks for Single-Step-Fabricated Field-Effect Transistors: The Importance of Postdeposition Ligand Removal. *ACS Appl. Mater. Interfaces* **2018**, *10* (6), 5626–5632.

(47) Talapin, D. V; Murray, C. B. PbSe Nanocrystal Solids for N- and P-Channel Thin Film Field-Effect Transistors. *Science (80-.).* **2005**, *310* (5745), 86 LP-89.

(48) K., Z.; Ramalingom, P. A. D.; M., T.; D., N.; K., B.; W., C.; H., B.; K., C. V. S.; C., K.; V., K. Synthesis and Characterization of PbTe Thin Films by Atomic Layer Deposition. *Phys. status solidi* **2014**, *211* (6), 1329–1333.

(49) Bala, M.; Bhogra, A.; Khan, S. A.; Tripathi, T. S.; Tripathi, S. K.; Avasthi, D. K.; Asokan, K. Enhancement of Thermoelectric Power of PbTe Thin Films by Ag Ion Implantation. *J. Appl. Phys.* **2017**, *121* (21), 215301.

(50) Sumirat, I.; Ando, Y.; Shimamura, S. Theoretical Consideration of the Effect of Porosity on Thermal Conductivity of Porous Materials. *J. Porous Mater.* **2006**, *13* (3), 439–443.

(51) Martin, J.; Nolas, G. S.; Zhang, W.; Chen, L. PbTe Nanocomposites Synthesized from PbTe Nanocrystals. *Appl. Phys. Lett.* **2007**, *90* (22), 222112.

(52) Johnsen, S.; He, J.; Androulakis, J.; Dravid, V. P.; Todorov, I.; Chung, D. Y.; Kanatzidis, M. G. Nanostructures Boost the Thermoelectric Performance of PbS. *J. Am. Chem. Soc.* **2011**, *133* (10), 3460–3470.

(53) Zhang, K.; Zhang, Q.; Wang, L.; Jiang, W.; Chen, L. Enhanced Thermoelectric Performance of Se-Doped PbTe Bulk Materials via Nanostructuring and Multi-Scale Hierarchical Architecture. *J. Alloys Compd.* **2017**, *725*, 563–572.

(54) Roh, J. W.; Jang, S. Y.; Kang, J.; Lee, S.; Noh, J.-S.; Kim, W.; Park, J.; Lee, W. Size-Dependent Thermal Conductivity of Individual Single-Crystalline PbTe Nanowires. *Appl. Phys. Lett.* **2010**, *96* (10), 103101.

(55) Kim, M.-S.; Lee, W.-J.; Cho, K.-H.; Ahn, J.-P.; Sung, Y.-M. Spinodally Decomposed PbSe-PbTe Nanoparticles for High-Performance Thermoelectrics: Enhanced Phonon Scattering and Unusual Transport Behavior. *ACS Nano* **2016**, *10* (7), 7197–7207.